Limitation of TCA Cycle Intermediates Represents an Oxygen-Independent Nutritional Antibacterial Effector Mechanism of Macrophages

Graphical Abstract
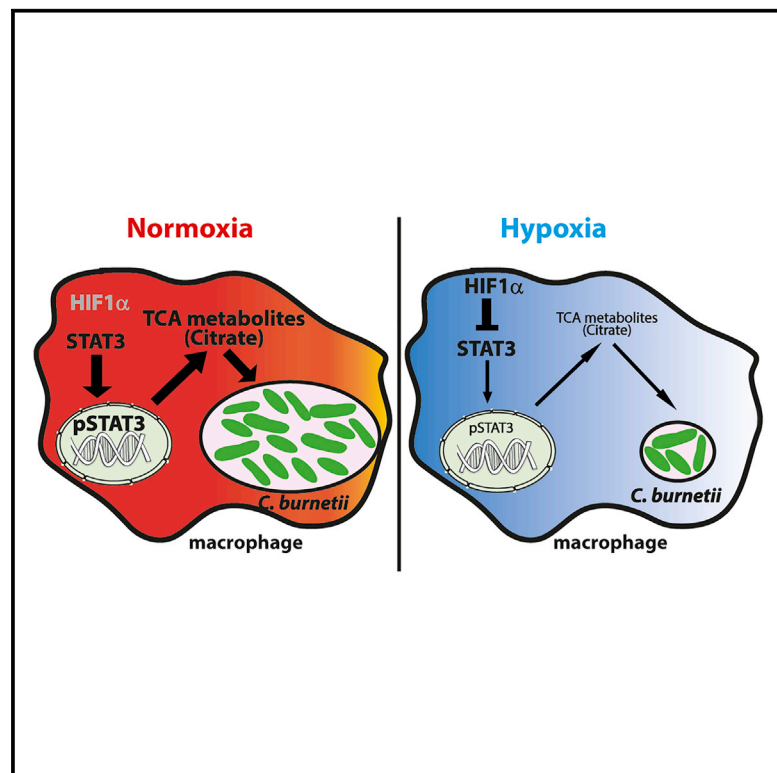
Authors

Inaya Hayek, Fabian Fischer, Jan Schulze-Luehrmann, ..., Stefan Wirtz, Jonathan Jantsch, Anja Lührmann

Correspondence

jonathan.jantsch@ukr.de (J.J.), anja.luehrmann@uk-erlangen.de (A.L.)

In Brief

The mechanisms that control bacterial infection under hypoxic conditions are only partially understood. Hayek et al. show that hypoxia-mediated stabilization of HIF1α results in the inhibition of STAT3 activation and the reduction of TCA metabolite levels, including citrate, in macrophages. This prevents *C. burnetii* replication without reducing bacterial viability.

Highlights

- Hypoxia curtails *C. burnetii* replication in macrophages without reducing bacterial viability

- Hypoxia induces robust HIF1α accumulation in infected macrophages

- HIF1α reduces STAT3 activation and citrate availability in infected hypoxic macrophages

- Low levels of TCA metabolites impede *C. burnetii* replication in macrophages

Limitation of TCA Cycle Intermediates Represents an Oxygen-Independent Nutritional Antibacterial Effector Mechanism of Macrophages

Inaya Hayek,[1,7] Fabian Fischer,[1,2,7] Jan Schulze-Luehrmann,[1,7] Katja Dettmer,[3] Katharina Sobotta,[4] Valentin Schatz,[5] Lisa Kohl,[1] Katharina Boden,[4] Roland Lang,[1] Peter J. Oefner,[3] Stefan Wirtz,[6] Jonathan Jantsch,[5,*] and Anja Lührmann[1,8,*]

[1]Mikrobiologisches Institut, Universitätsklinikum Erlangen, Friedrich-Alexander-Universität (FAU) Erlangen-Nürnberg, 91054 Erlangen, Germany
[2]Klinik für Innere Medizin I, Universitätsklinikum Regensburg, 93053 Regensburg, Germany
[3]Institut für Funktionelle Genomik, Universität Regensburg, 93053 Regensburg, Germany
[4]Institut für Medizinischen Mikrobiologie, Universitätsklinikum Jena, 07743 Jena, Germany
[5]Institut für Klinische Mikrobiologie und Hygiene, Universitätsklinikum Regensburg, Universität Regensburg, 93053 Regensburg, Germany
[6]Medizinische Klinik 1, Universitätsklinikum Erlangen, Friedrich-Alexander-Universität (FAU) Erlangen-Nürnberg, 91052 Erlangen, Germany
[7]These authors contributed equally
[8]Lead Contact
*Correspondence: jonathan.jantsch@ukr.de (J.J.), anja.luehrmann@uk-erlangen.de (A.L.)
https://doi.org/10.1016/j.celrep.2019.02.103

SUMMARY

In hypoxic and inflamed tissues, oxygen (O_2)-dependent antimicrobial defenses are impaired due to a shortage of O_2. To gain insight into the mechanisms that control bacterial infection under hypoxic conditions, we infected macrophages with the obligate intracellular pathogen *Coxiella burnetii*, the causative agent of Q fever. Our experiments revealed that hypoxia impeded *C. burnetii* replication in a hypoxia-inducible factor (HIF) 1α-dependent manner. Mechanistically, under hypoxia, HIF1α impaired the activity of STAT3, which in turn reduced the intracellular level of TCA cycle intermediates, including citrate, and impeded *C. burnetii* replication in macrophages. However, bacterial viability was maintained, allowing the persistence of *C. burnetii*, which is a prerequisite for the development of chronic Q fever. This knowledge will open future research avenues on the pathogenesis of chronic Q fever. In addition, the regulation of TCA cycle metabolites by HIF1α represents a previously unappreciated mechanism of host defense against intracellular pathogens.

INTRODUCTION

O_2 levels of <1%, which can be found in inflamed and infected tissues, are known to incapacitate key antimicrobial and immunomodulating effector enzymes such as indoleamine 2,3-dioxygenase, phagocyte oxidase, and type 2 nitric oxide (NO) synthase (NOS2), which depend on oxygen (O_2) as a substrate (Jantsch and Schödel, 2015). Nevertheless, bacterial infections can be controlled in the absence of O_2-dependent antimicrobial defense (Campbell et al., 2014). Enhanced expression of antimicrobial peptides (Peyssonnaux et al., 2005) may fulfill this

task in part and restrain the replication of pathogens, until tissue O_2 levels normalize and O_2-dependent antimicrobial effectors such as nicotinamide adenine dinucleotide phosphate-positive (NADPH) oxidase (PHOX) or NOS2 kick in (Jantsch and Schödel, 2015). However, additional defense strategies are likely to contribute to the control of infection under hypoxic conditions. We hypothesized that the limitation of metabolites that are essential for the proliferation of pathogens may function as an antimicrobial effector mechanism in inflamed hypoxic tissue.

To test this hypothesis, we resorted to *Coxiella burnetii*, an obligate intracellular pathogen and the causative agent of the zoonotic disease Q fever (Maurin and Raoult, 1999). It is able to withstand hypoxic conditions, and its replication in macrophages is only in part controlled by O_2-dependent defense mechanisms, as NOS2 and PHOX contribute to the control of *C. burnetii* replication in macrophages, but macrophage lacking NOS2 and PHOX are still able to control *C. burnetii* infection (Brennan et al., 2004; Zamboni and Rabinovitch, 2003). In addition, *C. burnetii* requires hypoxic conditions for axenic replication (Omsland et al., 2009). However, whether hypoxia is also required for intracellular replication within the *C. burnetii*-containing vacuole (CCV) is unknown.

Acute Q fever often presents as a mild flu-like illness, but interstitial pneumonia or hepatitis can also be seen. The infection can become chronic months or years after primary infection. Chronic Q fever mainly manifests as endocarditis and is potentially fatal (Maurin and Raoult, 1999). Interleukin 10 (IL-10) is overproduced by the monocytes of patients with chronic Q fever (Honstettre et al., 2003) and impairs the killing of *C. burnetii* in human macrophages (Ghigo et al., 2001), indicating a role for IL-10 in chronic Q fever. The immunomodulatory cytokine IL-10 deactivates macrophages through signal transducer and activator of transcription 3 (STAT3)-dependent signaling. However, the role of STAT3 during *C. burnetii* infection has not been studied yet.

Here, we report hypoxia-induced hypoxia-inducible factor 1α (HIF1α) reduces the intracellular availability of Krebs cycle
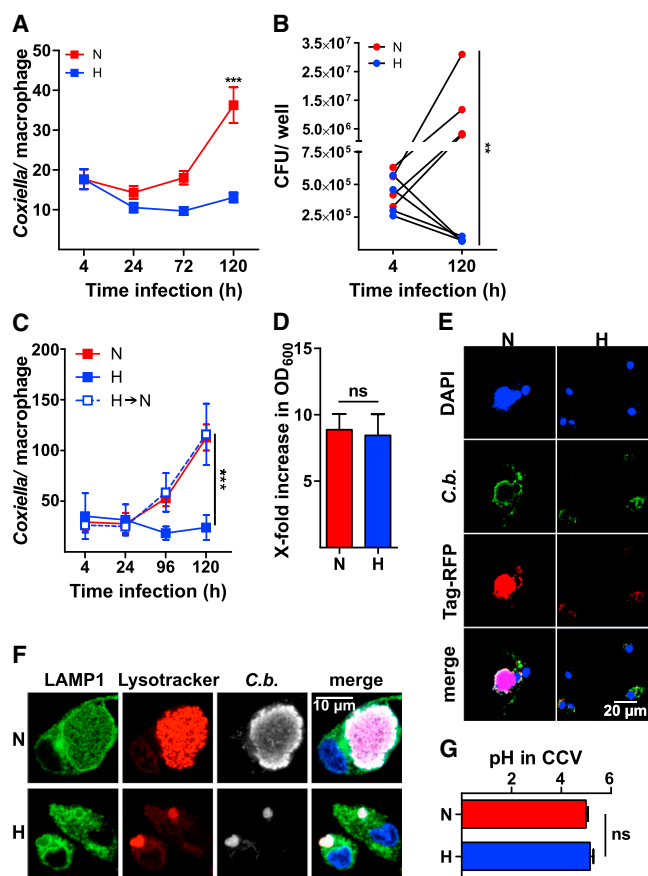
Figure 1. Hypoxia Impairs *C. burnetii* Replication in Macrophages
(A) Macrophages were infected with NMII for the times indicated under normoxia (N) or hypoxia (H). Bacterial load was assessed by qPCR. Means ± SEMs, n = 26, two-way ANOVA with Bonferroni post-test.
(B) Human MDM from four different donors was infected with NMII for 4 and 120 h under N or H. Bacterial numbers were determined by colony-forming unit (CFU) counts. n = 4, Friedman test with Dunn's post-test.
(C) Macrophages were infected with NMII for the times indicated under N, H, or re-oxygenation after 48 h of H (H→N). Bacterial load was assessed by qPCR. Means ± SEMs, n = 4, two-way ANOVA with Bonferroni post-test.
(D) After 120 h, bacteria were purified and cultured in ACCM-2 for 72 h. Bacterial replication was assessed by optical density 600 (OD_{600}) measurement. Means ± SEMs, n = 5, Mann-Whitney U test.
(E) Macrophages were infected with NMII harboring an IPTG-inducible RFP plasmid. At 120 h post-infection, IPTG was added for 8 h and the cells were fixed and stained with DAPI and an antibody against *C. burnetii*. One of 3 experiments with similar results is shown.
(F) At 120 h post-infection, LysoTracker Red was added, and the cells were stained with DAPI and with antibodies against LAMP1 and *C. burnetii*. One of 3 experiments with similar results is shown.
(G) At 48 h post-infection, LysoSensor dye was added, and the vacuolar pH was measured in at least 40 CCVs in two independent experiments. Means ± SEMs, t test.
*p < 0.05, **p < 0.01, ***p < 0.001, and ns, p > 0.05.

intermediates citrate, succinate, and itaconate in macrophages in a STAT3-dependent manner, thereby impairing the growth but not the survival of *C. burnetii* in macrophages.

RESULTS

Hypoxia Prevents *C. burnetii* Replication

To test whether hypoxia may induce O_2-independent antimicrobial control measures, we infected macrophages with *C. burnetii* Nine Mile phase II (NMII) under normoxia or hypoxia and determined the number of bacteria per macrophage by qRT-PCR of the *C. burnetii* *dotA* and the mouse *Alb1* genes. Replication of NMII was observed only under normoxia (Figure 1A), suggesting that hypoxia impeded bacterial replication. Human monocyte-derived macrophages (hMDM) also allowed NMII replication only under normoxic conditions (Figure 1B). To evaluate whether NMII is killed by hypoxic macrophages, we reoxygenated infected hypoxic macrophages, which led to the renewed replication of NMII (Figure 1C). Next, we lysed infected macrophage at 120 h post-infection to isolate and cultivate NMII in acidified citrate cysteine medium-2 (ACCM-2). As shown in Figure 1D, NMII replicated equally well, regardless of whether it was isolated from normoxic or hypoxic macrophages, indicating that hypoxic macrophages restricted NMII replication without killing the pathogen. To verify this assumption, we used NMII carrying a plasmid with isopropyl β-D-1-thiogalactopyranoside (IPTG)-inducible Tag-red fluorescent protein (RFP). Macrophages infected for 120 h with NMII were treated with IPTG, and the expression of Tag-RFP was visualized by confocal microscopy. Under both normoxia and hypoxia, NMII was able to synthesize Tag-RFP (Figure 1E), thus confirming that NMII remained viable in hypoxic macrophages. These results were surprising, as *C. burnetii* requires hypoxic conditions for axenic replication, indicating that not O_2 per se, but O_2-mediated alterations, are essential for the observed phenotype.

Hypoxia Does Not Prevent Maturation of the CCV

C. burnetii requires a phagolysosomal-like compartment for replication (Howe et al., 2010; Schulze-Luehrmann et al., 2016). This prompted us to characterize the CCV. By using lysosomal-associated membrane protein 1 (LAMP-1) and LysoTracker Red to label lysosomal compartments, we found CCVs positive for LAMP1 and LysoTracker Red under both culture conditions. However, the CCVs in hypoxic macrophages were much smaller (Figure 1F). Similarly, regardless of the available O_2, CCVs were positive for DQ Red BSA, a dye that produces bright fluorescence only upon hydrolysis by proteases, indicating that the CCV is a lysosomal-like compartment with degradative activity under both hypoxic and normoxic conditions (Figures S1A and S1B). Since replication of *C. burnetii* requires a pH of 4.0–5.0 (Hackstadt and Williams, 1981), we determined the pH of the CCVs. At 48 h post-infection, it was ∼5.0 under both normoxia and hypoxia (Figure 1G). Thus, the control of bacterial replication in hypoxic macrophages is not mediated by an altered phagosome maturation process.

Reduced IL-10 Secretion under Hypoxia Does Not Explain the Inhibition of *C. burnetii* Replication

Given that the cytokine IL-10 is known to suppress important antimicrobial effector functions and to facilitate *C. burnetii* replication in macrophages (Bogdan et al., 1991; Meghari et al., 2008), we analyzed IL-10 in the supernatant of NMII-infected
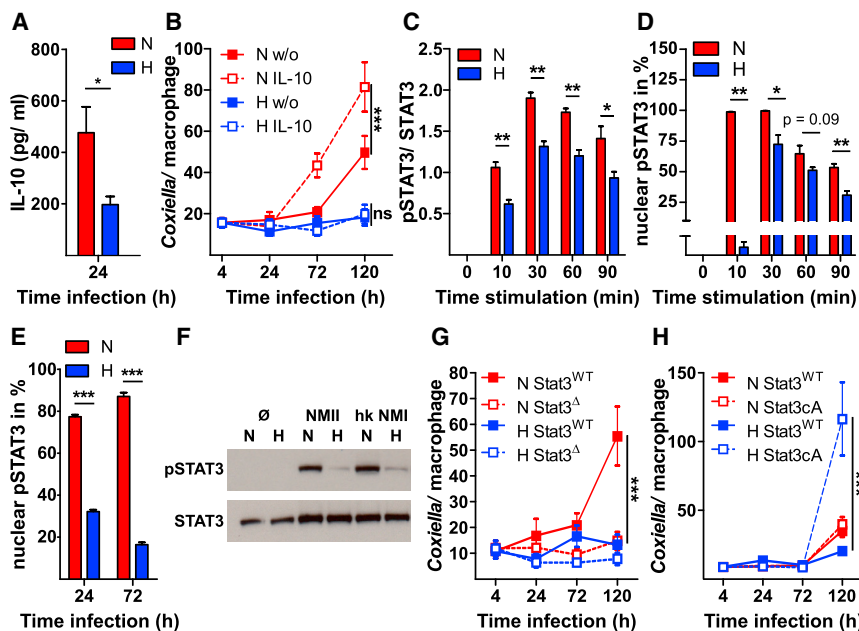
Figure 2. STAT3 Signaling Is Essential for *C. burnetii* Replication in Macrophages

(A) At 24 h post-infection, IL-10 levels were analyzed by ELISA. Means ± SEMs, n = 14, t test.

(B) Infected macrophages were stimulated with 20 ng/mL IL-10. Bacterial load was analyzed by qPCR. Means ± SEMs, n = 10.

(C and D) Uninfected cells were stimulated with (C) 0.5 ng/mL or (D) 20 ng/mL IL-10. (C) Ratio of phosphorylated STAT3 (pSTAT3) to total STAT3 was analyzed by immunoblot. Means ± SEMs, n = 3, t test. (D) Nuclear translocation of pSTAT3 was assessed by confocal microscopy. 200 cells from 3 independent experiments were analyzed. Means ± SEMs, n = 5, t test or Mann-Whitney *U* test.

(E) In at least 100 infected macrophages nuclear pSTAT3 was assessed by confocal microscopy. Means ± SEMs, n = 3, t test.

(F) Macrophages not infected or infected with NMII or heat-killed NMI for 24 h were subjected to immunoblot analysis using antibodies against pSTAT3 and STAT3. One representative immunoblot from three independent experiments is shown.

(G) STAT3-deficient (STAT3$^{\Delta}$) and wild-type (STAT3^{WT}) macrophages were infected. Bacterial load was assessed by qPCR. Means ± SEMs, n = 6.

(H) Macrophages with constitutively active STAT3 (STAT3cA) and wild-type (STAT3^{WT}) macrophages were infected. Bacterial load was assessed by qPCR. Means ± SEMs, n = 8.

(B, G, and H) Two-way ANOVA with Bonferroni post hoc test.

*p < 0.05, **p < 0.01, ***p < 0.001, and ns, p > 0.05.

macrophages. Secretion of IL-10 by infected hypoxic macrophages was reduced (Figure 2A). However, the addition of IL-10 failed to restore the replication of NMII in hypoxic macrophages, while it boosted the growth of NMII in normoxic macrophages (Figure 2B). Thus, the hypoxia-induced reduction of IL-10 secretion only partially explains the inhibition of *C. burnetii* replication. Therefore, we hypothesized that hypoxia may specifically interfere with IL-10 signaling.

Activation of STAT3 Is Crucial for *C. burnetii* Replication

IL-10 signals via the Janus kinase 1 (JAK1)/STAT3 pathway (Murray, 2006). The activation of this pathway leads to STAT3 phosphorylation and translocation into the nucleus (Yu et al., 2014). The addition of IL-10 to normoxic macrophages induced the phosphorylation of STAT3 within 10 min. Under hypoxia, the phosphorylation of STAT3 was reduced (Figures 2C and S1C). This difference was even more pronounced for the subcellular localization of phosphorylated STAT3 (pSTAT3). Ten minutes after the addition of IL-10 to normoxic macrophages, pSTAT3 was detectable in nearly 100% of the nuclei, while hardly any hypoxic macrophages showed nuclear pSTAT3 (Figures 2D and S1D). Similarly, the nuclear localization of pSTAT3 was reduced in NMII-infected macrophages under hypoxia (Figure 2E). NMII, a biosafety level 2 organism, is avirulent in immunocompetent mice. It was established in embryonated eggs by the serial passage of phase I *C. burnetii* NM, a virulent pathogen and a biosafety level 3 bacteria, which resulted in severely truncated lipopolysaccharides (LPSs) (Howe et al., 2010). Infection with heat-killed NMI resulted in the reduced phosphorylation of

STAT3 under hypoxia (Figures 2F and S1E), suggesting that the observed phenotype may also be applicable to NMI and does not depend on LPS length.

Infection of hMDM with NMII only induced potent phosphorylation of STAT3 under normoxia (Figure S1F). These data suggested that hypoxia impaired the activation of STAT3. Therefore, we analyzed the role of STAT3 in *C. burnetii* replication by studying the outcome of *C. burnetii* infection in STAT3-deficient (STAT3$^{\Delta}$) or constitutively active STAT3 (STAT3cA) macrophages and their respective wild-type controls (STAT3^{WT}). Under normoxia, *C. burnetii* was only able to replicate in WT and in STAT3cA macrophages, but not in STAT3$^{\Delta}$ macrophages (Figures 2G and 2H), demonstrating that STAT3 activity is essential for *C. burnetii* replication. Of note, in STAT3cA macrophages, there was a pronounced *C. burnetii* replication under hypoxia (Figure 2H). These data suggest that the hypoxia-induced impairment of STAT3 activation and not the lack of O_2 itself prevents the proliferation of *C. burnetii* in hypoxic macrophages.

HIF1α and STAT3 Differently Regulate *C. burnetii* Replication

HIF1α, the key regulator of cellular hypoxic responses, is known to interfere with STAT3 signaling (Jiang et al., 2013). In addition, HIF1α has been recognized to control key microbicidal functions of immune cells, as it is involved in phagocytosis and bacterial killing (Palazon et al., 2014). Therefore, we analyzed HIF1α levels. At 24 h post-infection, neither uninfected nor NMII or heat-killed NMI-infected macrophages showed robust stabilization of HIF1α in the presence of ample O_2. However, hypoxia induced

(G) Macrophages were infected with NMII under N with or without the addition of DPI at the times indicated. Bacterial load was assessed at 120 h post-infection by qPCR. Means ± SEMs, n = 3, one-way ANOVA with Tukey post-test.
*p < 0.05, **p < 0.01, ***p < 0.001, and ns, p > 0.05.

prominent HIF1α accumulation, which was further augmented upon infection (Figures 3A and S2A). Similar results were obtained from NMII-infected hMDM (Figure S2B). We hypothesized that hypoxia-induced HIF1α accumulation may account for the impaired activation of STAT3 and the lack of *C. burnetii* replication. To address this, we analyzed the nuclear localization of pSTAT3 in HIF1α-deficient (HIF1α^Δ) and controls (HIF1α^WT) macrophages upon stimulation with IL-10. Under normoxia, pSTAT3 was translocated into the nucleus within 10 min, regardless of the HIF1α status (Figure 3B). In contrast, hypoxia delayed and reduced the nuclear localization of pSTAT3 in WT macrophages (Figures 3B and S2C). In HIF1α^Δ macrophages, this hypoxia-induced impairment of pSTAT3 translocation was abrogated (Figures 3B and S2C). Similarly, the hypoxia-induced impairment of pSTAT3 translocation was partially abolished in NMII-infected HIF1α^Δ macrophages exposed to hypoxic conditions (Figure 3C). These data suggest that HIF1α hampered the activation of STAT3. To confirm this, we used pharmacological agents to alter HIF1α or STAT3 activity. Treatment with dimethyloxallyl glycine (DMOG) under normoxia led to HIF1α stabilization and reduced STAT3 activation. In contrast, stattic inhibited the phosphorylation of STAT3 under normoxia without influencing HIF1α stabilization (Figures 3D, 3E, and S2D).

From these findings, we predicted that NMII would replicate in macrophages lacking HIF1α under hypoxic conditions. As shown in Figure 3F, this is indeed the case. Thus, our data suggest that hypoxia suppresses STAT3 activation via HIF1α and thereby prevents the replication of NMII. NMII replication under hypoxia in HIF1α^Δ and STAT3cA macrophages exceeds the

replication under normoxia. To test whether this may be due to the impaired activity of O2-dependent defense mechanisms, we treated NMII-infected macrophages with diphenyleneiodonium (DPI), which is an inhibitor of the O2-dependent antimicrobial effector enzymes NOS2 and PHOX. Treatment with DPI increased the replication rates of NMII under normoxia (Figure 3G). This conforms to findings that NOS2 and PHOX are involved in the control of *C. burnetii* (Brennan et al., 2004; Zamboni and Rabinovitch, 2003) and supports our assumption that the increased *C. burnetii* replication under hypoxia in HIF1α^Δ and STAT3cA macrophages may be due to the shortage of O2, which represents a critical substrate for the antimicrobial effector enzymes NOS2 and PHOX.

HIF1α and STAT3 Differently Regulate the Intracellular Citrate Level

Recently, it was shown that STAT3 elevates the intracellular citrate level (Li et al., 2017) by facilitating Slc13a5-dependent citrate uptake (von Loeffelholz et al., 2017) and by promoting the expression of citrate synthase (MacPherson et al., 2017), which suggests that STAT3 may shift metabolism toward oxidative phosphorylation. In contrast, the lack of O2 and the consequent stabilization of HIF1α caused a switch from oxidative phosphorylation to anaerobic glycolysis (Kelly and O'Neill, 2015). Hypoxia led to a metabolic shift toward anaerobic glycolysis during *C. burnetii* infection, as indicated by the increased levels of lactate and the reduced amounts of the Krebs cycle intermediates citrate, succinate, and *cis*-aconitate-derived itaconate (Figures 4A and S3). However, in both HIF1α^Δ macrophages
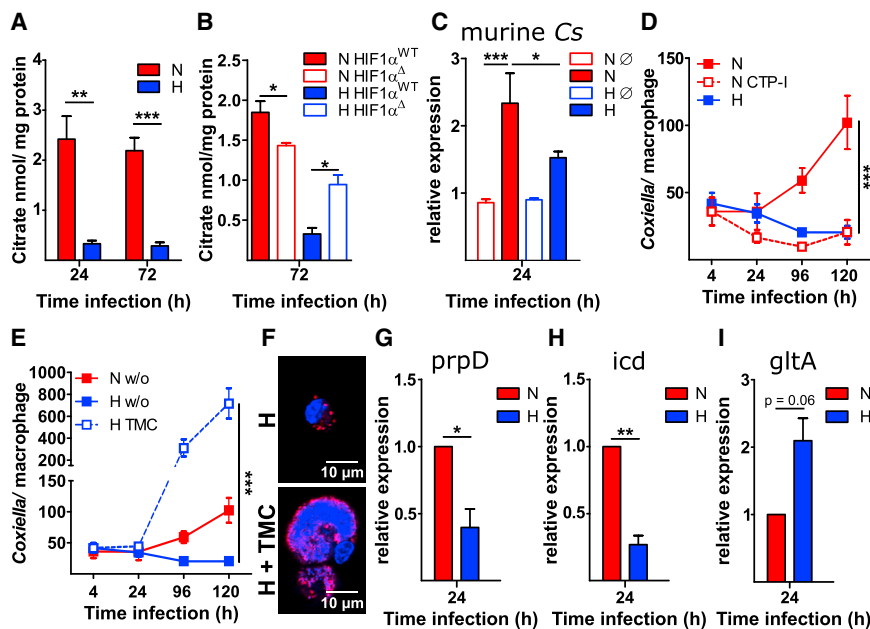
Figure 4. The HIF1α and STAT3 Contrariwise Regulate Intracellular Citrate Levels, and Thereby NMII Replication

(A) Citrate was extracted from infected cells and determined by liquid chromatography-tandem mass spectrometry (LC-MS/MS). Means ± SEMs, n = 3, t test.

(B) Intracellular citrate levels in macrophages deficient for HIF1α (HIF1α^Δ) or wild-type controls (HIF1α^{WT}). Means ± SEMs, n = 3, t test.

(C) Gene expression of murine citrate synthase was determined by qRT-PCR. The data are shown as means ± SEMs of ΔΔCT values (using hypoxanthine phosphoribosyltransferase [HPRT] as a calibrator), two-way ANOVA with Bonferroni post-test. n = 3.

(D) Infected macrophages were treated with 0.1 μM CTP inhibitor (CTP-I) or left untreated. The bacterial load was assessed by qPCR. Means ± SEMs, n = 6, two-way ANOVA with Bonferroni post hoc test.

(E and F) Infected macrophages were treated with 1 mM trimethylated citrate (TMC). (E) The bacterial load was assessed by qPCR or (F) cells were stained with DAPI (blue) and an antibody against *C. burnetii* (red). Means ± SEMs, n = 6, two-way ANOVA with Bonferroni post hoc test.

(G–I) Gene expression of *C. burnetii* 2-methylcitrate dehydratase (prpD) (G), isocitrate dehydrogenase (icd) (H), and citrate synthase (gltA) (I) was determined by qRT-PCR. Means ± SEMs of ΔΔCT values (using IS1111 as a calibrator), one-sample t test. n = 3.
*p < 0.05, **p < 0.01, ***p < 0.001, and ns, p > 0.05.

(Figure 4B) and STAT3cA macrophages (Figure S2E), but not in STAT3^Δ macrophages (Figure S2F), hypoxia failed to reduce citrate levels, indicating that HIF1α antagonized STAT3-induced Krebs cycle intermediate availability in infected macrophages under hypoxia. Under normoxia, neither HIF1α deficiency nor STAT3 deficiency resulted in altered citrate levels (Figures 4B and S2F), suggesting the neither HIF1α nor STAT3 controls metabolic processes in the presence of ample O$_2$.

In the following, we concentrated on the investigation of the role of citrate as one example of an HIF1α- and STAT3-regulated metabolite. Thus, to identify a possible underlying mechanism for the decreased availability of citrate under hypoxia, we analyzed the mRNA expression level of the murine citrate synthase (*Cs*). We detected an infection-dependent upregulation of *Cs*. However, under hypoxia, the expression of *Cs* was reduced (Figure 4C), supporting our conclusion that HIF1α antagonizes STAT3-induced activities. The upregulation of *Cs* may cause the observed increase in citrate levels during infection (Figure S3).

The axenic growth medium, which allows extracellular *C. burnetii* replication, contains high levels of citrate. If impaired replication of *C. burnetii* under hypoxia were due to a reduction in citrate levels, then pharmacological inhibition of the mitochondrial citrate transport protein (CTP) should abolish bacterial replication. The addition of CTP inhibitor prevented NMII replication under normoxia (Figure 4D), suggesting that mitochondrial function and mitochondrial-derived metabolites play an important role in *C. burnetii* replication. Next, we asked whether supplementation of hypoxic NMII-infected macrophages with citrate abrogates the inhibition of replication. Thus, NMII-infected hyp-

oxic macrophages were treated with trimethylated citrate (TMC), a membrane-permeable form of citrate. Treatment with TMC led to the strong replication of NMII under hypoxia (Figures 4E and 4F). Whether this is a direct or indirect effect of TMC must be determined. These data indicate that hypoxia impedes STAT3 activation via HIF1α and thereby reduces the intracellular availability of citrate and containment of *C. burnetii*.

In addition to the increased expression of the host cell citrate synthase during *C. burnetii* infection (Figure 4C), we observed that the bacterium adjusts the transcription of its own genes involved in citrate metabolism. Thus, the expression of proteins consuming citrate was downregulated under hypoxia (Figures 4G and 4H), while the expression of proteins participating in the production of citrate was upregulated (Figure 4I).

The HIF1α-STAT3-Citrate Axis Is Functional in *Legionella pneumophila*-Infected Macrophages

Next, we analyzed whether the HIF1α-STAT3-citrate axis is also operational during infection with *L. pneumophila*, the etiological agent of Legionnaires' pneumonia. We used *L. pneumophila* *ΔflaA*, a flagellin-deficient strain, which does not induce Toll-like receptor 5 (TLR5) and MyD88 signaling (Bartfeld et al., 2009). Hypoxia prevents the replication of *L. pneumophila* *ΔflaA* (Figures S4A and S4B), indicating that hypoxia-induced inhibition of bacterial replication is not *C. burnetii* specific. The infection of macrophages with *L. pneumophila* also induced potent phosphorylation of STAT3 under normoxia (Figure S4C). In addition, *L. pneumophila*-infected macrophages did not show robust stabilization of HIF1α in the presence of ample O$_2$. However, hypoxia triggered prominent HIF1α stabilization

that was augmented by infection (Figure S4D). Furthermore, infection with *L. pneumophila* resulted in the upregulation of citrate only in the presence of ample O_2 (Figure S4E). In contrast to the situation during *C. burnetii* infection, neither genetic ablation of HIF1α nor treatment with CTP inhibitor (CTP-I) or TMC rescued *L. pneumophila* replication (Figures S4F and S4G). These experiments demonstrate that although the HIF1α-STAT3-citrate axis is operational during *L. pneumophila* infection, neither HIF1α nor citrate is decisive for *L. pneumophila* intracellular replication.

DISCUSSION

O_2 availability in the microenvironment has a critical impact on immune responses (Jantsch and Schödel, 2015; Taylor and Colgan, 2017). The key transcription factor regulating O_2 homeostasis is HIF1α (Fuhrmann and Brüne, 2017). Here, we provide evidence that hypoxia restrains the intracellular growth of *C. burnetii* by limiting intracellular citrate levels (Figures 1A, 1B, 4A, 4D, and 4E). However, suppression of bacterial replication by the reduction of tricarboxylic acid (TCA) cycle intermediates did not lead to the elimination of *C. burnetii* in macrophages. Instead, the bacteria persisting in hypoxic macrophages remained fully viable (Figures 1C–1E). Our discovery that this state of persistence was elicited by hypoxia via the induction of HIF1α (Figure 3F), the suppression of STAT3 (Figures 2G and 2H), and the restriction of TCA cycle metabolites (Figures 4A and S3) establishes a hitherto unknown link between the tissue microenvironment and the host cell metabolism, which is of principal relevance for the understanding of pathogen control and evasion. Our data suggest that citrate depletion is critically involved in this state of affairs. However, it is unclear whether citrate depletion on its own or alterations in host and/or pathogen metabolism induced by citrate limitation mediate the restriction of *C. burnetii* replication.

Information about the trigger(s) and site(s) of *C. burnetii* persistence is rare. Our results suggest that *C. burnetii*, although contained, may persist in hypoxic tissues. Previous reports suggested that *C. burnetii* may hide either in the bone marrow (BM) or in adipose tissue (Bechah et al., 2014; Harris et al., 2000). As O_2 levels in the BM of rodents range from 0.6% to 2.8% O_2 (Spencer et al., 2014), the BM may provide a niche that facilitates the persistence of *C. burnetii*. Similarly, *Mycobacteria tuberculosis* survives within granulomas, in which hypoxia induces a state of dormancy (Belton et al., 2016; Wayne and Hayes, 1996).

Infection with various pathogens and macrophage stimulation with pathogen-associated molecular patterns (PAMPs) results in the accumulation of HIF1α, even in the presence of ample O_2. Normoxic HIF1α stabilization requires nuclear factor (NF)-κB activation (Rius et al., 2008) and involves transcriptional and posttranslational signaling events (Tannahill et al., 2013). Several studies have demonstrated that the accumulation of HIF1α is required to promote innate antimicrobial defenses (Palazon et al., 2014).

However, under normoxic conditions, *C. burnetii* fails to induce this inflammatory HIF1α activation (Figures 3A, S2A, and S2B), suggesting that *C. burnetii* has evolved strategies

to prevent hypoxia-independent HIF1α activation. In contrast, *M. tuberculosis* infection leads to an increase in HIF1α protein level and to a switch toward aerobic glycolysis under normoxia (Shi et al., 2015). Similarly, infection with *Chlamydia trachomatis* and *Anaplasma phagocytophilum* results in a metabolic shift toward aerobic glycolysis, which is linked to HIF1α (Cabezas-Cruz et al., 2017; Rother et al., 2018). In agreement with the above-mentioned ability of *C. burnetii* to prevent HIF1α stabilization on its own in the presence of O_2, we only detect a switch toward glycolysis during NMII infection under hypoxia (Figure S3).

STAT3 signaling is essential for the anti-inflammatory response (Murray, 2006). Recent evidence demonstrates that STAT3 is also involved in metabolism, as it controls the expression of the citrate transporter Slc13a5 (von Loeffelholz et al., 2017) and citrate synthase (MacPherson et al., 2017). In line with these findings, we found that the increased expression of citrate synthase correlates with increased STAT3 activity (Figure 4C). HIF1α, in contrast, facilitates the switch from oxidative phosphorylation to glycolysis and inhibits the Krebs cycle (Kelly and O'Neill, 2015). This leads to reduced levels of acetyl coenzyme A (CoA), which cannot be processed to citrate any longer (Kim et al., 2006). Overall, both STAT3 and HIF1α regulate the intracellular citrate level, but in opposite directions. Accordingly, we found that during *C. burnetii* and *L. pneumophila* infection, STAT3 activity increased the intracellular citrate level, while HIF1α activity prevented the elevation of citrate levels. This regulatory system is only operational under hypoxia, but not under normoxia.

Citrate, the first intermediate of the Krebs cycle, plays an important role in immunity. For instance, citrate is required for fatty acid biosynthesis, which is involved in mounting an appropriate immune response (Moon et al., 2015). Moreover, citrate can be converted via *cis*-aconitate to itaconate, which possesses antimicrobial and anti-inflammatory potential (Michelucci et al., 2013). Thus, citrate is thought to form a building block for the production of inflammatory mediators and antimicrobial molecules. However, high levels of citrate may also entertain the proliferation of *C. burnetii* (Omsland et al., 2008), which is likely to counteract the positive effects of citrate on microbial defense. Citrate is not only important in immunity but also in cancer, as it provides an important source of carbon (Hatzivassiliou et al., 2005; Mycielska et al., 2018). Of note, several cancers are characterized by HIF1α stabilization, which impedes citrate production through oxidative metabolism. Thus, there are remarkable parallels in the regulation of cellular metabolism in immunity and cancer with respect to citrate limitation. However, tumor cells may escape citrate limitation by the use of the reductive carboxylation pathway (Wise et al., 2011); *C. burnetii* is apparently unable to compensate for this limitation.

Not only the infection with *C. burnetii* and *L. pneumophila* (Figure S3) but also the infection with *Chlamydia trachomatis* caused an increase in citrate levels (Rother et al., 2018), suggesting that bacterial sensing by the host cell may induce a switch in metabolism to fight against invading pathogens. However, in contrast to *L. pneumophila*, *C. burnetii* may require citrate for replication, suggesting that this host cell defense

mechanism is counterproductive during *C. burnetii* infection. How *C. burnetii* benefits from citrate is unknown at present. It was shown that *Staphylococcus aureus* is able to sense host cell citrate and subsequently to adjust the expression of virulence genes in addition to metabolism (Ding et al., 2014). It remains to be elucidated whether host cell levels of citrate do indeed not only affect the expression of metabolic genes (Figures 4G–4I) but also of virulence factors.

In conclusion, we have demonstrated that under hypoxia, HIF1α prevents the activation of STAT3 in macrophages, which in turn results in the reduced availability of the Krebs cycle intermediates succinate, itaconate, and citrate. The lack of these TCA cycle metabolites is linked to the shutdown of *C. burnetii* replication, while it simultaneously induces a state of persistence, which may be important for the establishment of chronic Q fever. These findings demonstrate that the regulation of TCA cycle metabolites by innate HIF1α signaling represents a principle of nutritional pathogen containment under hypoxia.

STAR★METHODS

Detailed methods are provided in the online version of this paper and include the following:

- KEY RESOURCES TABLE
- CONTACT FOR REAGENT AND RESOURCE SHARING
- EXPERIMENTAL MODEL AND SUBJECT DETAILS
  - Mice
  - Murine bone marrow derived macrophages
  - Human peripheral blood derived macrophages
  - Coxiella burnetii
  - Legionella pneumophila
- METHOD DETAILS
  - Cell culture
  - Infection
  - Treatment with chemicals
  - DNA purification
  - Quantification of C. burnetii load
  - Colony-forming units
  - Analysis of IL-10
  - RNA
  - STAT3 immunoblot
  - HIF1α immunoblot
  - Immunofluorescence
  - TagRFP assay
  - Ratiometric pH measurements
  - GC-MS
- QUANTIFICATION AND STATISTICAL ANALYSIS

SUPPLEMENTAL INFORMATION

Supplemental Information can be found with this article online at https://doi.org/10.1016/j.celrep.2019.02.103.

ACKNOWLEDGMENTS

AUTHOR CONTRIBUTIONS

A.L. and J.J. conceived the study. A.L., F.F., I.H., J.S.-L., J.J., S.W., K.D., and P.J.O. designed the study. F.F., J.S.-L., I.H., K.D., and K.S. performed the experiments. A.L., J.J., F.F., J.S.-L., I.H., and K.D. analyzed the data. A.L., J.J., S.W., K.D., P.J.O., L.K., R.L., K.B., and V.S. provided resources. A.L. and J.J. supervised the study and provided critical advice. A.L., J.J., P.J.O., F.F., J.S.-L., and I.H. wrote the manuscript.

DECLARATION OF INTERESTS

The authors declare no competing interests.

REFERENCES

Bartfeld, S., Engels, C., Bauer, B., Aurass, P., Flieger, A., Brüggemann, H., and Meyer, T.F. (2009). Temporal resolution of two-tracked NF-kappaB activation by *Legionella pneumophila*. Cell. Microbiol. *11*, 1638–1651.

Bechah, Y., Verneau, J., Ben Amara, A., Barry, A.O., Lépolard, C., Achard, V., Panicot-Dubois, L., Textoris, J., Capo, C., Ghigo, E., and Mege, J.L. (2014). Persistence of *Coxiella burnetii*, the agent of Q fever, in murine adipose tissue. PLoS One *9*, e97503.

Belton, M., Brilha, S., Manavaki, R., Mauri, F., Nijran, K., Hong, Y.T., Patel, N.H., Dembek, M., Tezera, L., Green, J., et al. (2016). Hypoxia and tissue destruction in pulmonary TB. Thorax *71*, 1145–1153.

Bogdan, C., Vodovotz, Y., and Nathan, C. (1991). Macrophage deactivation by interleukin 10. J. Exp. Med. *174*, 1549–1555.

Brennan, R.E., Russell, K., Zhang, G., and Samuel, J.E. (2004). Both inducible nitric oxide synthase and NADPH oxidase contribute to the control of virulent phase I *Coxiella burnetii* infections. Infect. Immun. *72*, 6666–6675.

Cabezas-Cruz, A., Alberdi, P., Valdés, J.J., Villar, M., and de la Fuente, J. (2017). *Anaplasma phagocytophilum* Infection Subverts Carbohydrate Metabolic Pathways in the Tick Vector, *Ixodes scapularis*. Front. Cell. Infect. Microbiol. *7*, 23.

Campbell, E.L., Bruyninckx, W.J., Kelly, C.J., Glover, L.E., McNamee, E.N., Bowers, B.E., Bayless, A.J., Scully, M., Saeedi, B.J., Golden-Mason, L., et al. (2014). Transmigrating neutrophils shape the mucosal microenvironment through localized oxygen depletion to influence resolution of inflammation. Immunity *40*, 66–77.

Clausen, B.E., Burkhardt, C., Reith, W., Renkawitz, R., and Förster, I. (1999). Conditional gene targeting in macrophages and granulocytes using LysMcre mice. Transgenic Res. *8*, 265–277.

Dettmer, K., Nürnberger, N., Kaspar, H., Gruber, M.A., Almstetter, M.F., and Oefner, P.J. (2011). Metabolite extraction from adherently growing mammalian cells for metabolomics studies: optimization of harvesting and extraction protocols. Anal. Bioanal. Chem. *399*, 1127–1139.

Ding, Y., Liu, X., Chen, F., Di, H., Xu, B., Zhou, L., Deng, X., Wu, M., Yang, C.G., and Lan, L. (2014). Metabolic sensor governing bacterial virulence in *Staphylococcus aureus*. Proc. Natl. Acad. Sci. USA *111*, E4981–E4990.

Fogli, L.K., Sundrud, M.S., Goel, S., Bajwa, S., Jensen, K., Derudder, E., Sun, A., Coffre, M., Uyttenhove, C., Van Snick, J., et al. (2013). T cell-derived IL-17 mediates epithelial changes in the airway and drives pulmonary neutrophilia. J. Immunol. *191*, 3100–3111.

Fuhrmann, D.C., and Brüne, B. (2017). Mitochondrial composition and function under the control of hypoxia. Redox Biol. *12*, 208–215.

Ghigo, E., Capo, C., Raoult, D., and Mege, J.L. (2001). Interleukin-10 stimulates *Coxiella burnetii* replication in human monocytes through tumor necrosis factor down-modulation: role in microbicidal defect of Q fever. Infect. Immun *69*, 2345–2352.

Hackstadt, T., and Williams, J.C. (1981). Biochemical stratagem for obligate parasitism of eukaryotic cells by *Coxiella burnetii*. Proc. Natl. Acad. Sci. USA *78*, 3240–3244.

Harris, R.J., Storm, P.A., Lloyd, A., Arens, M., and Marmion, B.P. (2000). Long-term persistence of *Coxiella burnetii* in the host after primary Q fever. Epidemiol. Infect. *124*, 543–549.

Hatzivassiliou, G., Zhao, F., Bauer, D.E., Andreadis, C., Shaw, A.N., Dhanak, D., Hingorani, S.R., Tuveson, D.A., and Thompson, C.B. (2005). ATP citrate lyase inhibition can suppress tumor cell growth. Cancer Cell *8*, 311–321.

Honstettre, A., Imbert, G., Ghigo, E., Gouriet, F., Capo, C., Raoult, D., and Mege, J.L. (2003). Dysregulation of cytokines in acute Q fever: role of interleukin-10 and tumor necrosis factor in chronic evolution of Q fever. J. Infect. Dis *187*, 956–962.

Howe, D., Shannon, J.G., Winfree, S., Dorward, D.W., and Heinzen, R.A. (2010). *Coxiella burnetii* phase I and II variants replicate with similar kinetics in degradative phagolysosome-like compartments of human macrophages. Infect. Immun. *78*, 3465–3474.

Jantsch, J., and Schödel, J. (2015). Hypoxia and hypoxia-inducible factors in myeloid cell-driven host defense and tissue homeostasis. Immunobiology *220*, 305–314.

Jiang, C., Kim, J.H., Li, F., Qu, A., Gavrilova, O., Shah, Y.M., and Gonzalez, F.J. (2013). Hypoxia-inducible factor 1α regulates a SOCS3-STAT3-adiponectin signal transduction pathway in adipocytes. J. Biol. Chem. *288*, 3844–3857.

Kelly, B., and O'Neill, L.A. (2015). Metabolic reprogramming in macrophages and dendritic cells in innate immunity. Cell Res. *25*, 771–784.

Kim, J.W., Tchernyshyov, I., Semenza, G.L., and Dang, C.V. (2006). HIF-1-mediated expression of pyruvate dehydrogenase kinase: a metabolic switch required for cellular adaptation to hypoxia. Cell Metab. *3*, 177–185.

Li, Z., Li, D., Choi, E.Y., Lapidus, R., Zhang, L., Huang, S.M., Shapiro, P., and Wang, H. (2017). Silencing of solute carrier family 13 member 5 disrupts energy homeostasis and inhibits proliferation of human hepatocarcinoma cells. J. Biol. Chem. *292*, 13890–13901.

Lührmann, A., Nogueira, C.V., Carey, K.L., and Roy, C.R. (2010). Inhibition of pathogen-induced apoptosis by a *Coxiella burnetii* type IV effector protein. Proc. Natl. Acad. Sci. USA *107*, 18997–19001.

MacPherson, S., Horkoff, M., Gravel, C., Hoffmann, T., Zuber, J., and Lum, J.J. (2017). STAT3 Regulation of Citrate Synthase Is Essential during the Initiation of Lymphocyte Cell Growth. Cell Rep. *19*, 910–918.

Maurin, M., and Raoult, D. (1999). Q fever. Clin. Microbiol. Rev. *12*, 518–553.

Meghari, S., Bechah, Y., Capo, C., Lepidi, H., Raoult, D., Murray, P.J., and Mege, J.L. (2008). Persistent *Coxiella burnetii* infection in mice overexpressing IL-10: an efficient model for chronic Q fever pathogenesis. PLoS Pathog. *4*, e23.

Michelucci, A., Cordes, T., Ghelfi, J., Pailot, A., Reiling, N., Goldmann, O., Binz, T., Wegner, A., Tallam, A., Rausell, A., et al. (2013). Immune-responsive gene 1 protein links metabolism to immunity by catalyzing itaconic acid production. Proc. Natl. Acad. Sci. USA *110*, 7820–7825.

Moon, J.S., Lee, S., Park, M.A., Siempos, I.I., Haslip, M., Lee, P.J., Yun, M., Kim, C.K., Howrylak, J., Ryter, S.W., et al. (2015). UCP2-induced fatty acid synthase promotes NLRP3 inflammasome activation during sepsis. J. Clin. Invest. *125*, 665–680.

Murray, P.J. (2006). Understanding and exploiting the endogenous interleukin-10/STAT3-mediated anti-inflammatory response. Curr. Opin. Pharmacol. *6*, 379–386.

Mycielska, M.E., Dettmer, K., Rümmele, P., Schmidt, K., Prehn, C., Milenkovic, V.M., Jagla, W., Madej, G.M., Lantow, M., Schladt, M., et al. (2018). Extracellular Citrate Affects Critical Elements of Cancer Cell Metabolism and Supports Cancer Development *In Vivo*. Cancer Res. *78*, 2513–2523.

Omsland, A., Cockrell, D.C., Fischer, E.R., and Heinzen, R.A. (2008). Sustained axenic metabolic activity by the obligate intracellular bacterium *Coxiella burnetii*. J. Bacteriol. *190*, 3203–3212.

Omsland, A., Cockrell, D.C., Howe, D., Fischer, E.R., Virtaneva, K., Sturdevant, D.E., Porcella, S.F., and Heinzen, R.A. (2009). Host cell-free growth of the Q fever bacterium *Coxiella burnetii*. Proc. Natl. Acad. Sci. USA *106*, 4430–4434.

Ostrop, J., Jozefowski, K., Zimmermann, S., Hofmann, K., Strasser, E., Lepenies, B., and Lang, R. (2015). Contribution of MINCLE-SYK Signaling to Activation of Primary Human APCs by Mycobacterial Cord Factor and the Novel Adjuvant TDB. J. Immunol. *195*, 2417–2428.

Palazon, A., Goldrath, A.W., Nizet, V., and Johnson, R.S. (2014). HIF transcription factors, inflammation, and immunity. Immunity *41*, 518–528.

Peyssonnaux, C., Datta, V., Cramer, T., Doedens, A., Theodorakis, E.A., Gallo, R.L., Hurtado-Ziola, N., Nizet, V., and Johnson, R.S. (2005). HIF-1alpha expression regulates the bactericidal capacity of phagocytes. J. Clin. Invest. *115*, 1806–1815.

Rius, J., Guma, M., Schachtrup, C., Akassoglou, K., Zinkernagel, A.S., Nizet, V., Johnson, R.S., Haddad, G.G., and Karin, M. (2008). NF-kappaB links innate immunity to the hypoxic response through transcriptional regulation of HIF-1alpha. Nature *453*, 807–811.

Rother, M., Gonzalez, E., Teixeira da Costa, A.R., Wask, L., Gravenstein, I., Pardo, M., Pietzke, M., Gurumurthy, R.K., Angermann, J., Laudeley, R., et al. (2018). Combined Human Genome-wide RNAi and Metabolite Analyses Identify IMPDH as a Host-Directed Target against Chlamydia Infection. Cell Host Microbe *23*, 661–671.e8.

Schatz, V., Strüssmann, Y., Mahnke, A., Schley, G., Waldner, M., Ritter, U., Wild, J., Willam, C., Dehne, N., Brüne, B., et al. (2016). Myeloid Cell-Derived HIF-1α Promotes Control of Leishmania major. J. Immunol. *197*, 4034–4041.

Schulze-Luehrmann, J., Eckart, R.A., Ölke, M., Saftig, P., Liebler-Tenorio, E., and Lührmann, A. (2016). LAMP proteins account for the maturation delay during the establishment of the *Coxiella burnetii*-containing vacuole. Cell. Microbiol. *18*, 181–194.

Shi, L., Salamon, H., Eugenin, E.A., Pine, R., Cooper, A., and Gennaro, M.L. (2015). Infection with *Mycobacterium tuberculosis* induces the Warburg effect in mouse lungs. Sci. Rep. *5*, 18176.

Spencer, J.A., Ferraro, F., Roussakis, E., Klein, A., Wu, J., Runnels, J.M., Zaher, W., Mortensen, L.J., Alt, C., Turcotte, R., et al. (2014). Direct measurement of local oxygen concentration in the bone marrow of live animals. Nature *508*, 269–273.

Takeda, K., Kaisho, T., Yoshida, N., Takeda, J., Kishimoto, T., and Akira, S. (1998). Stat3 activation is responsible for IL-6-dependent T cell proliferation through preventing apoptosis: generation and characterization of T cell-specific Stat3-deficient mice. J. Immunol. *161*, 4652–4660.

Tannahill, G.M., Curtis, A.M., Adamik, J., Palsson-McDermott, E.M., McGettrick, A.F., Goel, G., Frezza, C., Bernard, N.J., Kelly, B., Foley, N.H., et al. (2013). Succinate is an inflammatory signal that induces IL-1β through HIF-1α. Nature *496*, 238–242.

Taylor, C.T., and Colgan, S.P. (2017). Regulation of immunity and inflammation by hypoxia in immunological niches. Nat. Rev. Immunol. *17*, 774–785.

von Loeffelholz, C., Lieske, S., Neuschäfer-Rube, F., Willmes, D.M., Raschzok, N., Sauer, I.M., König, J., Fromm, M.F., Horn, P., Chatzigeorgiou, A., et al. (2017). The human longevity gene homolog INDY and interleukin-6 interact in hepatic lipid metabolism. Hepatology 66, 616–630.

Wayne, L.G., and Hayes, L.G. (1996). An in vitro model for sequential study of shiftdown of Mycobacterium tuberculosis through two stages of nonreplicating persistence. Infect. Immun. 64, 2062–2069.

Wise, D.R., Ward, P.S., Shay, J.E., Cross, J.R., Gruber, J.J., Sachdeva, U.M., Platt, J.M., DeMatteo, R.G., Simon, M.C., and Thompson, C.B. (2011). Hypoxia promotes isocitrate dehydrogenase-dependent carboxylation of α-ketoglutarate to citrate to support cell growth and viability. Proc. Natl. Acad. Sci. USA 108, 19611–19616.

Yu, H., Lee, H., Herrmann, A., Buettner, R., and Jove, R. (2014). Revisiting STAT3 signalling in cancer: new and unexpected biological functions. Nat. Rev. Cancer 14, 736–746.

Zamboni, D.S., and Rabinovitch, M. (2003). Nitric oxide partially controls Coxiella burnetii phase II infection in mouse primary macrophages. Infect. Immun. 71, 1225–1233.

STAR★METHODS

KEY RESOURCES TABLE

REAGENT or RESOURCE	SOURCE	IDENTIFIER
Antibodies		
Phospho-Stat3 (Tyr705) (D3A7) XP® Rabbit mAb	Cell Signaling Technology	Cat#9145; RRID: AB_2491009
Stat3 (D3Z2G) Rabbit mAb	Cell Signaling Technology	Cat#12640; RRID: AB_2629499
HIF-1α (C-Term) Polyclonal Antibody	Cayman Chemical	Cat#10006421; RRID: AB_10099184
Anti-Actin antibody produced in rabbit	Merck Sigma-Aldrich	Cat#A2066; RRID: AB_476693
Goat IgG anti-Rabbit IgG (H+L)-HRPO	Jackson ImmunoResearch Labs	Cat#111-035-045; RRID: AB_2337938
ProLong Diamond Antifade Mountant with DAPI	Invitrogen	Cat# P36971
C. burnetii rabbit antibody	Davids Biotechnology	N/A
C. burnetii mouse antibody	Davids Biotechnology	N/A
LAMP-1 (mouse) antibody	DSHB	Cat#1D4B; RRID: AB_2134500
Goat IgG anti-Mouse IgG (H+L)-Alexa Fluor 594	Jackson ImmunoResearch Labs	Cat#115-585-062; RRID:AB_2338876
Goat IgG anti-Rabbit IgG (H+L)-Alexa Fluor 488	Jackson ImmunoResearch Labs	Cat#111-545-045; RRID: AB_2338049
Goat IgG anti-Rat IgG (H+L)-Alexa Fluor 488	Jackson ImmunoResearch Labs	Cat#112-545-062; RRID:AB_2338356
Goat IgG anti-Rabbit IgG (H+L)-Alexa Fluor 594	Jackson ImmunoResearch Labs	Cat#111-585-045; RRID:AB_2338062
Bacterial and Virus Strains		
Coxiella burnetii NMII	Matteo Bonazzi	N/A
Coxiella burnetii NMII expressing IPTG-inducible TagRFP	This paper	N/A
Coxiella burnetii NMI	Katharina Boden	N/A
Legionella pneumophila ΔflaA	Lührmann et al., 2010	N/A
Biological Samples		
Human peripheral blood derived macrophages	Universitätsklinikum Erlangen	N/A
Chemicals, Peptides, and Recombinant Proteins		
CTP-I	Sigma-Aldrich	Cat#SML0068; CAS: 412940-35-3
Trimethyl citrate	Sigma-Aldrich	Cat#27502; CAS: 1587-20-8
Diphenyleneiodonium chloride	Sigma-Aldrich	Cat#D2926; CAS: 4673-26-1
DMOG	Sigma-Aldrich	Cat#D3695; CAS: 89464-63-1
Stat3 inhibitor V, stattic	Santa Cruz Biotechnology	Cat#202818; CAS: 19983-44-9
Dimethyl sulfoxide (DMSO)	Sigma-Aldrich	Cat# D5879; CAS: 67-68-5
Dithiothreitol (DTT)	AppliChem	Cat#A1101; CAS: 3483-12-3
2-Mercaptoethanol	Sigma-Aldrich	Cat#M3148; CAS: 60-24-2
Monensin	Alfa Aesar	Cat#J61669; CAS: 22373-78-0
Nigericin	Sigma-Aldrich	Cat#N7143; CAS: 28643-80-3
LysoTracker Red DND-99	Life Technologies	Cat#L7528
Lysosensor Yellow/Blue DND-160	Life Technologies	Cat# L7545
DQ-Red BSA	Life Technologies	Cat# D12051
IPTG	Thermo Scientific	Cat#R0392
Proteinase K, recombinant, PCR grade	Thermo Scientific	Cat# EO0492
5x QPCR MixEvaGreen® (Rox)	Bio & Sell	Cat#76.580.5000
QuantiFast SYBR Green PCR Kit	QIAGEN	Cat#204054
peqGOLD TriFast	Peqlab VWR	Cat#30-2010; CAS: 108-95-2, 593-84-0, 60-24-2
Recombinant Mouse IL-10 Protein	R&D systems	Cat#417-ML
Recombinant Human M-CSF	Peprotech	Cat#300-25

(Continued on next page)

Continued

REAGENT or RESOURCE	SOURCE	IDENTIFIER
Pierce ECL Western Blotting Substrate	Thermo Scientific	Cat#32106
cOmplete, Mini Protease Inhibitor Cocktail	Roche	Cat#04693124001
Paraformaldehyde, 16% w/v aq. soln., methanol free	Alfa Aesar	Cat#43368
SuperScript II Reverse Transcriptase	Invitrogen by Life Technologies	Cat#18064014
Sodium Pyruvate-13C3	Cambridge Isotopes	Cat#CLM-2440-0.5
Sodium-L-Lactate 13C3	Cambridge Isotopes	Cat#CLM-1578-0.25
Citric Acid-d4	Cambridge Isotopes	Cat#DLM-3487-PK
Fumaric Acid 13C4	Cambridge Isotopes	Cat#CLM-1529-0.1
Malic acid-2,3,3,-d3	CDN Isotopes	Cat#D-2122
Succinic Acid 13C4	Sigma Aldrich	Cat#293075
Glucose-U-13C	Eurisotop	Cat#CLM-1396-1
2X ACCM-2 Powder	Sunrise Science Products	Cat#4700-300
Horse serum	Cell Concepts	Cat#S-HEU 03-1; Charge CELC-13085
Fetal calf serum (FCS)	Biochrom	Cat#S0115; Lot: 1004B
Critical Commercial Assays		
Mouse IL-10 ELISA Set	BD Biosciences	Cat# 555252
RNase-Free DNase Set	QIAGEN	Cat#79254
FluoroProfile protein Quantification Kit	Sigma Aldrich	Cat#FP0010-1KT
Purple Protein Quantification Assay	Serva	Cat#39235.01
CD14 MicroBeads, human	Miltenyi Biotec	Cat#130-050-201
Experimental Models: Organisms/Strains		
Mouse: C57BL/6	Charles River	Strain Code: 027
Mouse: HIF1$\alpha^{\Delta myel}$	Jonathan Jantsch	N/A
Mouse: STAT3$^{\Delta myel}$	Stefan Wirtz	N/A
Mouse: STAT3cA^{myel}	Stefan Wirtz	N/A
Oligonucleotides		
mAlb1; Forward: GGCAACAGACCTGACCAAAG	This paper	N/A
mAlb1; Reverse: CAGCAACCAAGGAGAGCTTG	This paper	N/A
mHPRT; Forward: TCCTCCTCAGACCGCTTTT	This paper	N/A
mHPRT; Reverse: CCTGGTTCATCATCGCTAATC	This paper	N/A
mCS; Forward: GGACTGCATGGACCTCATTG	This paper	N/A
mCS; Reverse: CTGAGGGTCGGTGTAGCCTA	This paper	N/A
DotA; Forward: GCGCAATACGCTCAATCACA	Schulze-Luehrmann et al., 2016	N/A
DotA; Reverse: CCATGGCCCCAATTCTCTT	Schulze-Luehrmann et al., 2016	N/A
prpD; Forward: CCGATTATGTTGTCAATCATAAAATC GAGA	This paper	N/A
prpD; Reverse: CAAAATTGAAAGCAGCTTGCACCG	This paper	N/A
Icd; Forward: CTTACCAACACATCAAAGTTCCCAG	This paper	N/A
Icd; Reverse: CATCCATTCAATTTTTCGCTTTCCAGC	This paper	N/A
gltA; Forward:CAGTCGGTTGAATTTCCTATTTATTCAC	This paper	N/A
gltA; Reverse: CCATCGATAAAGGTAATTTTTGATTCA CAA	This paper	N/A
IS1111; Forward: AATTTCATCGTTCCCGGCAG	This paper	N/A
IS1111; Reverse: GCCGCGTTTACTAATCCCCA	This paper	N/A
Software and Algorithms		
Zen2009 software	Carl Zeiss	https://www.zeiss.de/mikroskopie/produkte/mikroskopsoftware/zen.html#downloads

(Continued on next page)

Continued

REAGENT or RESOURCE	SOURCE	IDENTIFIER
AxioVision 4.8	Carl Zeiss	https://www.micro-shop.zeiss.com/de/de/system/software+axio+vision-mehrfachlizenzen+biomed-axiovision+software/10226/
GraphPad Prism 5	GraphPad Software	https://www.graphpad.com/scientific-software/prism/

CONTACT FOR REAGENT AND RESOURCE SHARING

Further information and requests for resources and reagents should be directed to and will be fulfilled by the Lead Contact, Anja Lührmann (anja.luehrmann@uk-erlangen.de).

EXPERIMENTAL MODEL AND SUBJECT DETAILS

Mice

C57BL/6 wild-type mice were obtained from Charles River Breeding Laboratories (Sulzfeld, Germany). To obtain mice deficient in HIF1α in their myeloid cell compartment (HIF1$\alpha^{\Delta myel}$), *HIF1$\alpha^{flox/flox}$* mice were crossed with lysozyme M-driven Cre (LysM^{Cre})-transgenic mice (Clausen et al., 1999), both on a C57BL/6 background, as previously published (Schatz et al., 2016). C57BL/6 mice deficient in functional STAT3 (STAT3$^{\Delta myel}$) in the myeloid cell compartment were generated by crossing of LysM^{Cre} mice to STAT3^{flox} mice (Takeda et al., 1998). C57BL/6 mice with myleoid-specific constitutive activation of STAT3 (STAT3cA^{myel}), *R26Stat3C$^{stopfl/fl}$* mice (Fogli et al., 2013) were crossed with *LysM^{Cre}* mice. All mice utilized in this study were male animals at least six weeks of age.

Murine bone marrow derived macrophages

To generate primary bone marrow derived macrophages (MΦ), femoral and tibial bone marrow cavities were flushed. The cells were propagated in Teflon bags (Angst+Pfister, #01.1425.0130) containing Dulbecco's modified Eagle's medium (DMEM), 10% Fetal Calf Serum (FCS), 5% Horse Serum and 20% supernatant of L929 cells for 7-9 days at 37°C, 10% CO_2 and 21% O_2.

Human peripheral blood derived macrophages

Human peripheral blood was obtained from four healthy donors (Ethical Committee Erlangen approval number 111_12B). Donor 1 was a 42 year old male, donor 2 was a 62 year of male, donor 3 was a 26 year old female, donor 4 was a 38 year old male. Monocytes were obtained as described elsewhere (Ostrop et al., 2015). Briefly, PBMC were isolated from leukoreduction system chambers by density centrifugation. Monocytes were then positively selected using anti-CD14 microbeads (Miltenyi Biotec). For culture, RPMI 1640 medium was supplemented with 10% (v/v) FCS and penicillin/streptomycin. Monocytes were differentiated into macrophages using 50 U/ml M-CSF (Peprotech) at a density of 10 $\times$ 10^6 cells for 7 days without change of media at 37°C, 5% CO_2 and 21% O_2. Cells were washed with PBS, detached with accutase, carefully scraped off and pooled. Next, they were centrifuged, resuspended in RPMI-CM (described below), counted and seeded.

Coxiella burnetii

C. burnetii NMII strain clone 4 (RSA439) was generously provided by Matteo Bonazzi (CNRS Montpellier, France). *C. burnetii* NMII was propagated for 5 days in ACCM-2 at 37°C, 5% CO_2, and 2.5% O_2. *C. burnetii* NMII was heat killed at 70°C for 30 min under shaking at 500 rpm. *C. burnetii* NMI strain (RSA493) was heat killed at 70°C for 60 min under shaking at 500 rpm.

Legionella pneumophila

The flagellin-deficient strain of *L. pneumophila* flaA (ΔflaA) was used as described elsewhere (Lührmann et al., 2010). In short, from a single colony of *L. pneumophila*, a 2-days heavy patch was performed on a BCYE agar plate, which was incubated at 37°C, 5% CO_2, and 21% O_2.

METHOD DETAILS

Cell culture

Infected MΦ were cultured at 37°C, 5% CO_2, 21% O_2 (normoxia, N) or at 37°C, 5% CO_2, 0.5% O_2 (hypoxia, H). Hypoxic experiments were conducted in InvivO$_2$ hypoxic chamber (Baker Ruskinn, Bridgend, UK). Buffers and media were equilibrated for at least 4 h before usage in the hypoxic chamber.

Infection

MΦ were harvested, seeded and cultured at N in RPMI 1640 complete medium (RPMI-CM) containing 10% FCS, 1% HEPES and 0.5% β-mercaptoethanol. Prior to infection, *C. burnetii* were quantified by measuring the optical density at OD_{600}, where an OD_{600} of 1 equals 1×10^9 *C. burnetii*. The cells were infected with *C. burnetii* at MOI 10. Following infection, cells were centrifuged for 5 min at 250 x g and placed under N or H. After 4 h of infection, cells were washed with PBS and supplied with RPMI-CM.

Prior to infection with *L. pneumophila*, they were scraped off the plate, resuspended in PBS and then quantified by measuring the optical density at OD_{600}, where an OD_{600} of 1 equals 1×10^9 *L. pneumophila*.

Treatment with chemicals

After infection as described above, fresh RPMI-CM was added with or without the following chemicals. The mitochondrial citrate transport protein inhibitor (CTP-I) (SML0068, Sigma-Aldrich, Germany) was used at 0.1 μM. Trimethyl citrate (TMC) (27502, Sigma-Aldrich) was added at 1 mM. Stattic (STAT3 inhibitor V, #202818, Santa Cruz Biotechnology, USA), the control DMSO (D5879, Sigma-Aldrich), or the inhibitor DMOG (D3695, Sigma-Aldrich, Germany) were added at the indicated concentrations. Diphenyleneiodonium chloride (DPI) (D2926, Sigma-Aldrich), an inhibitor of NOS2 and PHOX, was used at 500 nM.

DNA purification

MΦ were detached using cell scrapers and pelleted at 500 x g for 10 min using a centrifuge pre-cooled to 4°C. Supernatent was removed and 500 μl lysis buffer (0.1 M EDTA, 100 mM NaCl, 10% SDS, 50 mM Tris-HCl pH 8.0) containing 0.2 mg/ ml Proteinase K were added. Cells were lysed over-night in a thermo shaker at 1000 rpm and 55°C. To remove cell detritus, reaction tubes were subsequently centrifuged 10 min at 20,000 x g and ambient temperature. Supernatants were transferred to new tubes and DNA in solution was precipitated by addition of 1 volume isopropanol (500 μl). DNA was pelleted at 20,000 x g and 4°C, washed two times with 1 mL 70% ethanol, and air-dried. Pellets were resuspended in 100 μl ultrapure H_2O.

Quantification of C. burnetii load

We defined the ratio of *C. burnetii* genomic copies to MΦ genomic copies as bacterial load per cell. *C. burnetii* genomes were quantified from isopropanol-precipitated DNA samples by qPCR with a primer set specific for the *dotA* gene. Purified *C. burnetii* NMII DNA in the range of 10^3 to 10^9 genome copies was used as template to generate standard curves (Schulze-Luehrmann et al., 2016). MΦ genomic copies were quantified from the same sample using a primer set specific for the murine *alb1* gene (exon 7). Isopropanol-purified DNA from 1×10^8 MΦ was diluted 10-fold down to 10 by serial dilution and served as a template to generate standard curves. qPCR was carried out with 5x QPCR MixEvaGreen (Rox) (Bio&Sell, Fürth, Germany), a 0.1 μM final concentration of each primer, and 2 μL isolated DNA (diluted 1:20 in ultrapure H_2O) as template in a final volume of 10 μL per reaction.

Colony-forming units

C. burnetii-infected human MΦ or *L. pneumophila*-infected MΦ were washed with PBS and lysed with ice-cold H_2O for 40 min. Next, the cells were pipetted repeatedly with a syringe carrying a 25G needle (25 G 1'' 0,5 × 25 mm, BD Microlance 3, Spain) to lyse the remaining cells. The suspension was then centrifuged for 10 min at 1000 rpm, 4°C. The supernatant was centrifuged for 1 min at 14000 rpm, 4°C. Next, the pellet was resuspended in 200 uL PBS pH 7.4. A serial dilution was performed and the diluted *C. burnetii* or *L. pneumophila* were pipetted in triplicates on ACCM-D/0.5% agarose plates or BCYE-agar plates, respectively. *C. burnetii*-plates were incubated for 2 weeks at 37°C, 5% CO_2 and 2.5% O_2 while *L. pneumophila* for 3 days at 37°C, 5% CO_2 and 21%O_2. CFUs were counted and calculated considering the dilution factors to meet the actual amount per one well.

Analysis of IL-10

Secretion of IL-10 by *C. burnetii* infected MΦ was measured in cell culture supernatants by ELISA (BD Biosciences, Heidelberg, Germany).

RNA

For each RNA sample, 2×10^6 infected MΦ were harvested at indicated time points. Medium was removed and cells were washed 1x with PBS. 1 mL peqGOLD TriFast (30-2010, Peqlab VWR, Belgium) was added to the wells. Homogenization, phase separation, RNA precipitation, RNA wash and RNA solubilization were performed according to the manufacturer's protocol. Pellets were resuspended in 50 μl RNase- free H_2O and stored at −80°C.

Isolated RNA were treated with DNase and RDD buffer (79254, QIAGEN, Hilden, Germany) for 10 min at 37°C. DNase was inactivated at 75°C for 5 min. Contamination with genomic DNA was checked via PCR and subsequent loading on a 2% agarose gel. No contamination was detected.

DNase-treated RNA was used to synthesize first strand cDNA using SuperScript II Reverse Transcriptase according to the manufacturer's protocol (18064-022, Invitrogen by Life Technologies, Carlsbad, USA).

qPCR was performed using the QuantiFast SYBR Green PCR Kit (204054, QIAGEN, Hilden, Germany), a 100 nM final concentration of each primer and 2 μL of 5-fold diluted cDNA as template in a final volume of 10 μL per reaction. Primers used for murine MΦ were Hprt1 (used as a housekeeping gene) and citrate synthase. Primers used for *C. burnetii* are IS1111 (used as a housekeeping

gene), 2-methylcitrate dehydratase prpD, NADP-dependent isocitrate dehydrogenase icd, and citrate synthase gltA. Primer sequences are listed in the key resources table. The quantification of the expression levels of the stated genes was referenced to the respective housekeeping gene and normalized to the mentioned normoxic sample. The $2^{-(\Delta\Delta CT)}$ method was used to calculate the fold change.

STAT3 immunoblot

For the IL-10 stimulated MΦ, MΦ were seeded and cultured for 2 h at 37°C, 5% CO_2, 21% O_2 (N) or at 0.5% O_2 (H). Next, the cells were stimulated with 0.5 ng / ml rmIL-10 (417-ML, R&D systems, Wiesbaden, Germany) for the indicated time points. MΦ, which were infected with *C. burnetii*, were prepared as explained before. Samples were washed with PBS and harvested with 2 x Laemmli SDS loading buffer (250 mM Tris-HCl pH 6.8, 8% SDS, 40% Glycerin, 8% β-mercaptoethanol, and 0.02% Bromophenol blue) and subsequently incubated for 5 min at 95°C, shaking at 450 rpm. Equal amounts of proteins were separated by SDS-PAGE and transferred to a PVDF membrane (Merck Millipore, Darmstadt, Germany). The membranes were probed with antibodies directed against pSTAT3 and STAT3 from Cell Signaling (Frankfurt, Germany). The proteins were visualized by using horseradish peroxidase-conjugated secondary antibodies (Dianova, Hamburg, Germany) and a chemiluminescence detection system (Thermo Fisher Scientific, Waltham, MA, USA).

HIF1α immunoblot

For probing HIF1α, the cells were lysed with 10 mM Tris-HCl pH 6.8, 6.65 M Urea, 10% Glycerin, 1% SDS with freshly added 1 mM DTT and complete proteinase inhibitory mix (Roche complete mini, EDTA free / Roche, Mannheim, Germany). Before loading equal amounts of proteins the lysed samples were adjusted with 4 x Laemmli SDS loading buffer and incubated for 8 min at 85°C, shaking at 450 rpm. The membranes were probed with antibodies directed against HIF1α (Cayman 10006421/ Biomol, Hamburg, Germany) and Actin (A 2066) from Merck Sigma-Aldrich (Darmstadt, Germany). The proteins were visualized by using horseradish peroxidase-conjugated secondary antibodies (Dianova, Hamburg, Germany) and a chemiluminescence detection system (Thermo Fisher Scientific, Waltham, MA, USA).

Immunofluorescence

For indirect immunofluorescence microscopy analyses, *C. burnetii* infected MΦ were cultured on 10mm coverslips in 24-well dishes. At indicated points of time, cells were fixed for 15 min with 4% paraformaldehyde (PFA), permeabilized 1 min with ice-cold methanol and quenched and blocked for 30 min with 50 mM NH_4Cl in PBS/ 5% goat serum (GS). After incubation with primary and secondary antibodies dilution in PBS/ 5% GS the coverslips were mounted using ProLong Diamond containing DAPI (Invitrogen). For visualization, a Carl Zeiss LSM 700 Laser Scan Confocal Microscope and the ZEN2009 software (Jena, Germany) were used.

In this study, we used primary antibodies directed against *C. burnetii*, LAMP-1 (Developmental Studies Hybridoma Bank, Iowa, IA, USA), and phosphorylated STAT3 (Cell Signaling, 9145). Secondary antibodies were Alexa Fluor labeled (Alexa Fluor 488 and 594) and purchased from Dianova, Hamburg, Germany. To detect acidic cell compartments, infected MΦ were incubated with equilibrated 1 μM LysoTracker Red DND-99 (Life Technologies) diluted in RPMI-CM one hour prior to fixation. As a phagolysosomal marker, DQ-Red BSA (Life Technologies) was used at a concentration of 2 μg/ml and incubated with the infected MΦ 4 hours prior to fixation.

TagRFP assay

To assess viability of intracellular *C. burnetii*, MΦ were infected with *C. burnetii* NMII strain harboring an IPTG-inducible TagRFP. At 120 h post-infection, 3 mM IPTG (ThermoFisher) was added. After an additional 8 h, cells were stained for indirect immunofluorescence microscopy as described.

Ratiometric pH measurements

One day prior to harvesting *C. burnetii* expressing IPTG-inducible TagRFP, 3 mM IPTG was added to the ACCM-2 medium. 1×10^6 MΦ were seeded in 35-mm glass bottom culture dishes (Mat Tek, Ashland, MA, USA). Cells were infected with *C. burnetii* expressing IPTG-inducible TagRFP at MOI 20 and cultured for 48 hours. Hypoxic samples were washed and incubated inside a hypoxic chamber that can be mounted on the ApoTome (Zeiss) and subsequently sealed air tight before image acquisition. After washing with equilibration buffer (5 mm NaCl, 115 mm KCl, 1.2 mm $MgSO_4$, 25 mm MES; pH 6.0) the cells were incubated in 2 μm Lysosensor Yellow/Blue DND-160 (Life Technologies) in equilibration buffer and life cell images were acquired between 1-15 min after addition of the dye with an ApoTome (Zeiss) and AxioVision 4.8 software. Cells were excited with 365 nM and the emission filters were 445 nM (B, less acidic) and 510 nM (Y; more acidic). Mean pixel values of fluorescence intensities of regions of interest (ROIs, 10 μm²) corresponding to CCVs (red fluorescence) were measured using AxioVision 4.8 software. Yellow to blue ratio of fluorescence intensities was further used to calculate vesicular pH employing the potential fit parameters from the calibration curve. To calibrate Lysosensor Yellow/Blue DND-160 emission ratios for a range of pH values *in situ*, cells were incubated before addition of the dual-wavelength fluorophore for 15 min with equilibration buffer of known pH (3.0-7.5) in the presence of 10 μM Monensin and 10 μM Nigericin. Monensin is a Na^+/H^+ antiporter whereas Nigericin is a K^+/H^+ antiporter, thus bringing the cytosol and CCVs to the pH of the surrounding medium. A standard curve was generated in GraphPad Prism to assign a predicted pH for relevant Y/B values.

An independent standard curve was generated on each experimental day. Yellow/blue values from duplicates of at least 19 individual cells in two independent experiments were averaged for the analysis.

GC-MS

Infected MΦ were lysed with ice-cold 80% methanol and frozen immediately at −80°C. During lysis, 10 μL of an internal standard solution containing $^{13}C_3$-lactate, $^{13}C_3$-pyruvate, $^{13}C_4$-succinate, $^{13}C_4$-fumarate, malate-d3, and citrate-d4 (1 mM each) was added. For further sample preparation, samples were thawed, vortexed, centrifuged (9560 x g, 6 min, 4°C) and the extract was collected. The cell pellet was washed twice with 80% methanol and the extracts were combined and dried in a vacuum evaporator (CombiDancer, Hettich AG, Bäch, Switzerland). Carboxylic acid analysis was performed by GC-MS after methoximation and silylation employing the derivatization protocol and instrumental setup recently described (Dettmer et al., 2011). An injection volume of 1 μL and splitless injection was used. Quantification was performed using a calibration curves with the stable isotope labeled compounds as internal standard. $^{13}C_4$-Fumarate was used as internal standard for itaconate. It should be noted that citrate and isocitrate are not chromatographically resolved by the employed method. But, the LLOQ for isocitrate is higher than for citrate and screening for a m/z value specific for isocitrate did not reveal noticeable detection of isocitrate. Intracellular metabolite amounts were normalized to protein amount. The protein pellet was lysed in a NaH_2PO_4 buffer (20 mM with 1.2% SDS) and the protein amount was measured using the FluoroProfile protein Quantification Kit (Sigma Aldrich, Taufkirchen, Germany) or the Purple Protein Quantification Assay (Serva).

QUANTIFICATION AND STATISTICAL ANALYSIS

Statistical analysis was conducted with Prism 5 (GraphPad software) and Excel (Microsoft). Statistical details can be found in the legends of the figures. Normality distribution was tested with D'Agostino & Pearson normality test or the Kolmogorov-Smirnov test, or, when N < 8, Shapiro-Wilk normality test or the Kolmogorov-Smirnov test. For non-normally distributed datasets, the Mann-Whitney test and Friedmann test with Dunns post-hoc test was used. Otherwise, two-way ANOVA with a Bonferroni post hoc test, one-way ANOVA with Tukey post hoc test, or the unpaired two-tailed Student's t test was used. The Welch's correction was used if unequal variances were detected. One-sample t-test was used when comparing datasets to normalized values. A value of p < 0.05 was considered significant.

Supplemental Information

Limitation of TCA Cycle Intermediates

Represents an Oxygen-Independent Nutritional

Antibacterial Effector Mechanism of Macrophages

Inaya Hayek, Fabian Fischer, Jan Schulze-Luehrmann, Katja Dettmer, Katharina Sobotta, Valentin Schatz, Lisa Kohl, Katharina Boden, Roland Lang, Peter J. Oefner, Stefan Wirtz, Jonathan Jantsch, and Anja Lührmann

Supplemental Figure 1
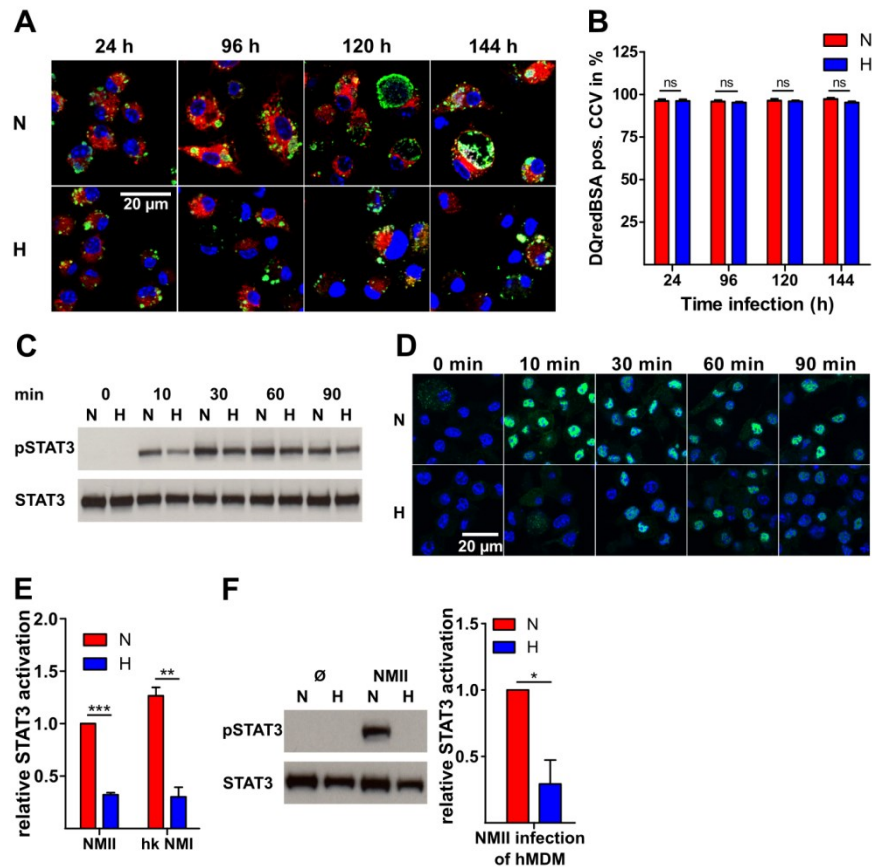
Fig. S1. Hypoxia does not prevent maturation of the CCV, but hampers STAT3 activation. Related to Figure 1 and 2. **(A-B)** MΦ were infected with NMII for the times indicated under both N and H. Four hours prior to fixation DQ-Red BSA (2µg/ml) was added. Cells were fixed and stained with DAPI (blue) and an antibody against *C. burnetii* (green). **(A)** One of 3 experiments with similar results is shown. **(B)** The number of DQ-Red BSA positive CCVs was counted in 100 infected cells per experiment. Mean ± SEM, n=3, t-test, ns=p>0.05. **(C-D)** Uninfected cells were stimulated with 0.5 ng/ml **(C)** or 20ng/ml **(D)** IL-10 for the times indicated under N and H. **(C)** STAT3 phosphorylation was analyzed by immunoblotting. One representative immunoblot is shown. **(D)** Nuclear translocation of pSTAT3 was assessed by confocal microscopy (DAPI (blue) and anti-pSTAT3 antibody (green)). **(E)** MΦ not infected or infected with NMII or heat-killed NMI for 24 h were subjected to immunoblot analysis using antibodies against pSTAT3 and STAT3. Ratio of phosphorylated STAT3 (pSTAT3) to total STAT3 is displayed. Mean ± SEM, n=3, t-test or one-sample t-test, **p<0.01. **(F)** Human MDM either not infected or infected with NMII for 24 h were subjected to immunoblot analysis using antibodies against pSTAT3 and STAT3. One representative immunoblot is shown. Ratio of phosphorylated STAT3 (pSTAT3) to total STAT3 is displayed. Mean ± SEM, n=3, one-sample t-test, *p<0.05.
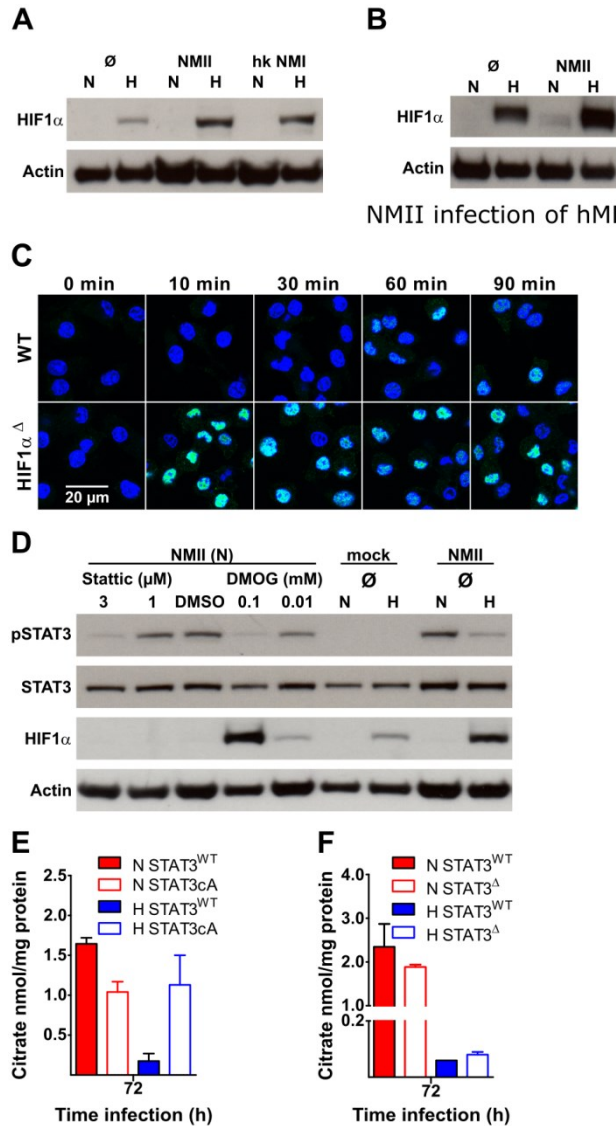
Fig. S2. HIF1α inhibits STAT3 activity. Related to Figure 3. **(A)** MΦ not-infected or infected with NMII or heat-killed NMI for 24 h under N or H were analyzed by immunoblot analysis using antibodies against HIF1α and Actin. One representative immunoblot is shown. **(B)** Human MDM either not infected or infected with NMII for 24 h were subjected to immunoblot analysis using antibodies against HIF1α and Actin. One representative immunoblot is shown. Ratio of HIF1α to Actin is displayed. Mean ± SEM, n=3, t-test, **p<0.01, *p<0.05. **(C)** Uninfected wild-type (WT) MΦ or MΦ deficient for HIF1α (HIF1α$^\Delta$) were stimulated with 20 ng/ml IL-10 under hypoxia for the times indicated. Cells were stained with DAPI (blue) and anti-pSTAT3 (Tyr705) antibody (green). **(D)** MΦ were either not infected or infected with NMII. Infected cells were either treated with stattic, DMOG, or with DMSO, as a control. At 24 h post infection/treatment STAT3 activity and HIF1α stability was analyzed by immunoblot analysis. One representative immunoblot is shown. **(E)** Citrate levels at 72 h post-infection in infected MΦ expressing constitutively active STAT3 (STAT3cA) versus wild-type controls (STAT3^{WT}). Mean ± SEM, n=2. **(F)** Citrate levels at 72 h post-infection in infected STAT3-deficient MΦ (STAT3$^\Delta$) versus wild-type controls (STAT3^{WT}). Mean ± SEM, n=3.

Supplemental Figure 3

		Normoxia			Hypoxia			
		1	2	3	1	2	3	p value
Pyruvate	Ø	1,45	1,64	2,22	1,1	1,32	1,81	0,31
	L. pneumophila	6,62	7,31	5,81	0,98	1,84	1,64	0,00
	C. burnetii	0,97	1,19	1,35	0,94	1,18	0,88	0,30
Lactate	Ø	8,51	12,19	10,18	27,82	41,42	38,35	0,00
	L. pneumophila	16,68	24,15	23,08	31,76	54,89	51,26	0,03
	C. burnetii	9,48	9,96	13,54	above ULOQ	30,04	29,17	0,00
Succinate	Ø	0,11	0,21	0,23	0,12	0,14	0,26	0,87
	L. pneumophila	4,07	4,64	3,56	0,32	0,96	0,98	0,00
	C. burnetii	3,28	3,36	3,06	0,43	0,5	0,45	0,00
Itaconate	Ø	0,23	0,42	0,27	0,13	0,11	0,15	0,04
	L. pneumophila	39,7	62,05	34,75	2,49	4,17	4,98	0,01
	C. burnetii	above ULOQ	42,23	43,55	16,62	18,96	14,35	0,00
Fumarate	Ø	0,57	0,8	0,63	0,45	0,66	0,8	0,82
	L. pneumophila	1,79	2,12	1,68	1,9	4,28	3,7	0,12
	C. burnetii	0,51	0,46	0,53	0,7	0,55	0,51	0,23
Malate	Ø	1,02	1,54	1,27	0,79	1,2	1,76	0,94
	L. pneumophila	4,57	6,03	4,79	4,96	12,63	10,81	0,14
	C. burnetii	1,49	1,81	1,92	1,68	1,7	1,57	0,54
Citrate	Ø	0,65	1,17	0,6	0,41	0,34	0,2	0,06
	L. pneumophila	2,55	2,84	1,81	0,43	0,62	0,39	0,00
	C. burnetii	2,19	1,52	2,11	0,47	0,49	0,4	0,00

untreated (Ø)
L. pneumophila (after 30 h)
C. burnetii (after 24 h)

0   (nmol/ mg protein)   60

Fig. S3. Hypoxia and bacterial infection leads to a metabolic shift. Related to Figure 4. MΦ were either not infected or infected with *L. pneumophila ΔflaA* or with *C. burnetii* for the times indicated under N and H. Carboxylic acids were analyzed by GS-MS. The amounts of the metabolites are shown in nmol/mg from three independent experiments. The amount of metabolites under hypoxia and normoxia were compared by t-test.

Supplemental Figure 4
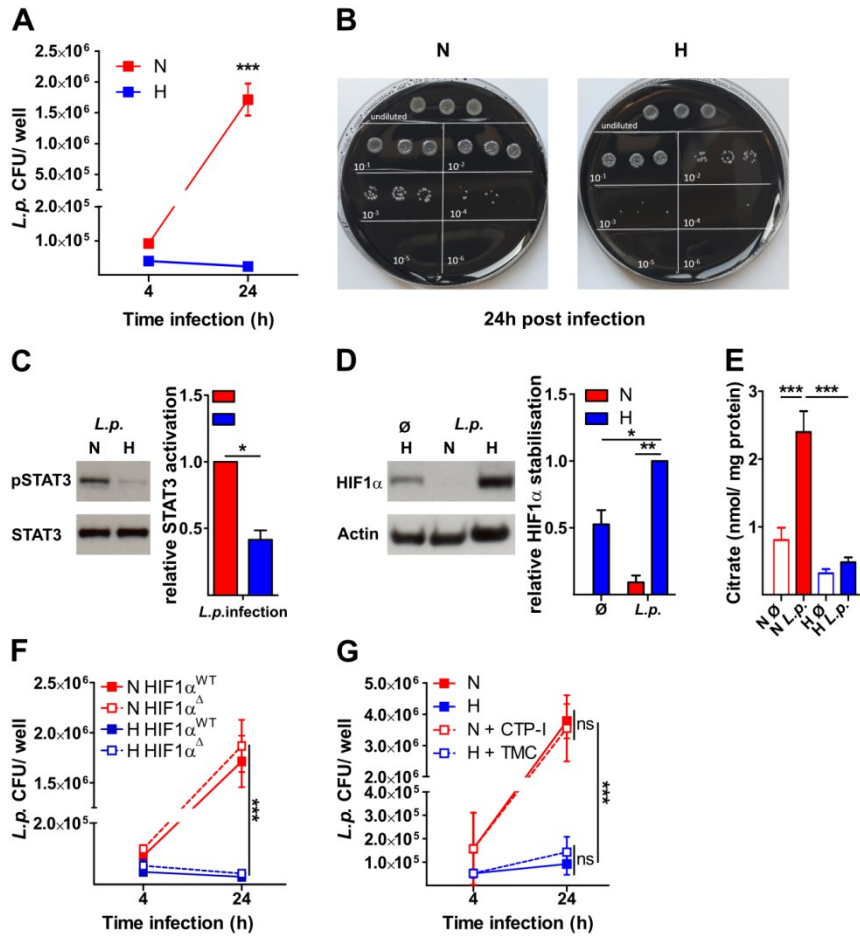
Fig. S4. The HIF1α-STAT3-citrate axis is functional, but dispensable during *L. pneumophila* infection. Related to Figure 1-4. **(A-B)** MΦ were infected with *L. pneumophila ΔflaA* for the times indicated under N and H. Bacterial numbers were determined by CFU counts. Mean ± SEM, n=3, two-way ANOVA with Bonferroni post-test, ***p<0.001. **(C)** MΦ infected with *L. pneumophila ΔflaA* for 18 h under N or H were analyzed by immunoblot analysis using antibodies against pSTAT3 and STAT3. One representative immunoblot is shown. Ratio of phosphorylated STAT3 (pSTAT3) to total STAT3 is displayed. Mean ± SEM, n=3, one-sample t-test, p*<0.05. **(D)** MΦ not infected or infected with *L. pneumophila ΔflaA* for 18 h under N or H were analyzed by immunoblot analysis using antibodies against HIF1α and Actin. One representative immunoblot is shown. Ratio of HIF1α to Actin is displayed. Mean ± SEM, n=3, one-sample t-test, **p<0.01, *p<0.05. **(E)** Citrate levels in not infected and *L. pneumophila ΔflaA* infected MΦ after 30 h of incubation. Mean ± SEM, n=3, two-way ANOVA with Bonferroni post-test. ***p<0.001. **(F)** MΦ deficient for HIF1α (HIF1α$^\Delta$) or from littermate controls (HIF1α^{WT}) were infected with *L. pneumophila ΔflaA* and CFU was determined. Mean ± SEM, n=3, two-way ANOVA with Bonferroni post-test, ***p<0.001. **(G)** *L. pneumophila ΔflaA* infected MΦ were treated with 0.1 μM CTP inhibitor (CTP-I), 1 mM trimethylated citrate (TMC) or left untreated. Bacterial load was assessed by CFU. Mean ± SEM, n=3, two-way ANOVA with Bonferroni post-test. ***p<0.001, ns=p>0.05.